



Dynamic Model for Magnetostrictive Systems With Applications to Damper Design

Zhangxian Deng[®], Qian Zhang, and Marcelo J. Dapino[®]

Abstract—Magnetostrictive iron-gallium alloys are able to dissipate mechanical energy via eddy currents and magnetic hysteresis. The mechanically induced eddy current loss is determined by the piezomagnetic coefficient; the hysteresis loss is usually quantified by the phase lag. This study first characterizes these losses for research grade, <100>-oriented, highly textured, polycrystalline Fe_{81.6}Ga_{18.4} within the structural frequency range (up to 800 Hz). The magnetic biasing is provided by applying a constant current of 500 mA on a pair of electromagnets; the mechanical excitation is a sinusoidal stress wave (3 \pm 0.2 MPa) superimposed on a -20 MPa constant stress. As stress frequency increases, the piezomagnetic coefficient decreases from 32.27 to 10.33 T/GPa and the phase lag $|\Delta \phi|$ increases from 11.38° to 43.87°. A rate-dependent finite element framework decoupling eddy current loss and hysteresis loss is then developed. The model accurately reproduces the experimental results in both quasi-static and dynamic regimes. Guided by the knowledge of material properties and the finite element model, a coil-less and solid-state damper is designed which can attenuate vibrations before they propagate and induce structure-borne noise and damage. Modeling results show that the loss factor of this damper can be continuously tuned from 0 to a maximum value of 0.107 by adjusting the precompression on the magnetostrictive component.

Index Terms—Eddy currents, hysteresis, magnetostrictive devices, vibration control.

I. INTRODUCTION

AGNETOSTRICTIVE materials, such as Terfenol-D and Galfenol, deform when exposed to magnetic field. The field-induced deformation, or magnetostriction, has motivated two active vibration attenuation strategies. The first strategy directly controls the magnetostriction to counteract structural vibrations [1]. The other strategy, which takes advantage of

Manuscript received July 25, 2017; revised December 5, 2017 and January 30, 2018; accepted May 6, 2018. Date of publication May 15, 2018; date of current version August 14, 2018. Recommended by Technical Editor W. Li. We wish to acknowledge the member organizations of the Smart Vehicle Concepts Center, a National Science Foundation Industry-University Cooperative Research Center (www.SmartVehicleCenter.org) supported by NSF Grant IIP-1738723. (Corresponding author: Marcelo J. Dapino.)

The authors are with the NSF IUCRC Smart Vehicle Concepts Center, Department of Mechanical and Aerospace Engineering, The Ohio State University, Columbus, OH 43210 USA (e-mail: deng.92@osu.edu; zhang.1704@buckeyemail.osu.edu; dapino.1@osu.edu).

Color versions of one or more of the figures in this paper are available online at http://ieeexplore.ieee.org.

Digital Object Identifier 10.1109/TMECH.2018.2836301

the magnetic-field-induced Young's modulus variation, actively switches magnetostrictive materials between their soft and stiff states [2]–[4].

Active vibration control is effective but requires external power sources and complex controllers. Passive vibration control that dissipates vibration energy through dampers is convenient. Magnetostrictive materials undergo magnetization change when mechanically stressed. The stress-induced magnetization, or Villari effect, has been implemented to develop shunted magnetostrictive dampers, which typically consist of magnetostrictive materials, coils, and electrical loads [5]-[8]. In those devices, mechanical vibration first induces varying magnetic flux density and the flux density variation is converted to electrical energy which is then dissipated as heat on attached electrical loads. Experimental results showed that the maximum loss factor available from a Terfenol-D-based shunted damper is 0.25 at 350 Hz [8]. Compared with viscoelastic materials, shunted magnetostrictive dampers have the advantage of being mechanically stiff. Hence, vibration energy can be attenuated at its source before it propagates and induces structure-borne noise. Recent studies have also elucidated that shunted magnetostrictive dampers can adapt themselves to environmental uncertainties and changing operating conditions, since their loss factors can be continuously tuned by adjusting the impedance of the shunted circuit [6], [9].

A disadvantage of shunted magnetostrictive dampers is that they require bulky coils and electrical circuits which are not convenient for certain applications. Previous studies have revealed that a solid-state magnetostrictive damper without coils and electrical circuits is possible due to magnetic hysteresis and mechanically induced eddy current loss [10], [11]. Magnetostrictive materials that exhibit high magnetic permeability and electrical conductivity, such as Galfenol, carbon-doped Galfenol, and Alfenol, are ideal candidates for this type of damper.

This study focuses on <100>-oriented, highly textured, polycrystalline $\mathrm{Fe_{81.6}\,Ga_{18.4}}$. Performance of the coil-less and solid-state damper is determined by the combined effect of magnetic hysteresis and eddy currents. Magnetic hysteresis, which is dominated by frequency-independent pinning site loss, has been characterized in the literature [12]. Eddy currents induced by dynamic mechanical excitation depend on material properties, including electrical conductivity, magnetic permeability, and piezomagnetic coefficient. The electrical conductivity of Galfenol is 1.18 MS/m [13], which is frequency-independent. The magnetic permeability and piezomagnetic coefficient are

defined as

$$\mu := \frac{\partial B}{\partial H} \quad \text{and} \quad d_{33}^I := \frac{\partial B}{\partial T} \tag{1}$$

respectively. Here, H and T are the input magnetic field and stress, respectively, B is the corresponding magnetic flux density measured at a given excitation current. Due to the magnetome-chanical coupling in Galfenol, μ and d_{33} depend on magnetic and mechanical excitations. The values of μ and d_{33} have been characterized in the quasi-static regime [11], [12], [14], [17]–[19]. Galfenol also exhibits frequency-dependent magnetic permeability and piezomagnetic coefficient due to its high electrical conductivity. Recent studies have measured the values of μ and d_{33} of Galfenol in the dynamic regime [16], [20].

The frequency-, stress-, and field-dependent magnetic permeability and piezomagnetic coefficient offer opportunities for adaptive damper design. However, tuning the performance of magnetostrictive devices requires an efficient and accurate material-level model that can describe both static and dynamic magnetostrictive behavior [21]-[23]. Most existing materiallevel models require a large number of unphysical parameters and are too impractical for design purposes. Several quasi-static and efficient material-level models, which are based on Gibbs energy expressions, are available for Galfenol in the literature [14], [17], [24]. Dynamic material-level models that incorporate frequency-dependent eddy current loss and magnetic hysteresis have been developed based on empirical expressions [7], [25]-[29]. This approach suffers from the disadvantage that empirical model parameters need to be identified through complicated experiments at various frequencies. Deng [30] recently developed a dynamic model for magnetostrictive materials by combining the energy-based material-level model with magnetic field diffusion equations. This model is only applicable to small input amplitudes when the magnetostrictive effect can be approximated by linear equations.

Besides the magnetostrictive element, a typical magnetostrictive damper also includes supporting components, such as permanent magnets, magnetic flux paths, and precompression mechanisms. Hence, a system-level model considering both active and passive elements is essential for damper design. Deng and Dapino [15] combined the static hysteresis of Galfenol with finite element frameworks and accurately reproduced the d_{33}^I response in the quasi-static regime. Zhao and Lord [31] developed a dynamic lumped parameter model and simulated the eddy current loss in a Terfenol-D rod. However, system-level models that simultaneously involve static hysteresis loss and dynamic eddy current loss have been lacking.

This study develops material-level and system-level models with a focus on magnetostrictive damper design. In Section II, modeling frameworks considering stress-induced eddy current losses and magnetic field diffusion are developed in COMSOL Multiphysics for magnetostrictive materials and magnetostrictive dampers, respectively. In Section III, the proposed model is validated up to 800 Hz using flux density versus stress measurements from a research grade, <100>-oriented, highly textured, polycrystalline $Fe_{81.6}Ga_{18.4}$. Based on the experimental results of d_{33}^I and the proposed system-level model, a conceptual design of coil-less and solid-state dampers

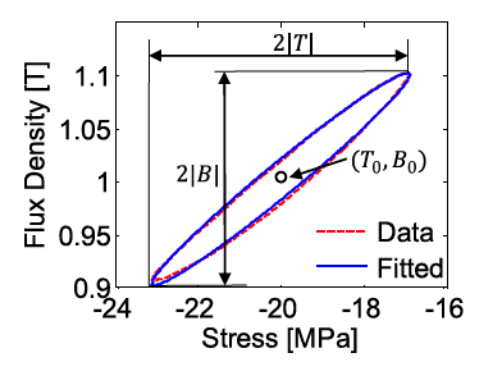


Fig. 1. Comparison of stress-flux density minor loops at 4 Hz: measurements (red dashed line) and fitted curve (blue solid line).

is presented, followed by detailed system optimization in Section IV.

II. THEORY

A. Calculation of Material Properties

1) Piezomagnetic Coefficient d_{33}^I : In previous quasi-static studies, d_{33}^I was calculated either by fitting a polynomial function [12] or by linear regression [19]. But none of these time-domain methods are suitable for dynamic characterization due to their sensitivities to measurement noise and input stress perturbation. To overcome the drawbacks associated with previous methods, this study quantifies the rate-dependent d_{33}^I in the frequency domain [32]. The sinusoidal input stress T_{33} with a frequency of f_0 in the frequency domain is

$$T = |T|e^{j\phi_T} + T_0 \tag{2}$$

where |T| is the stress amplitude, T_0 is the bias stress, and ϕ_T is the phase of the stress excitation. Since Galfenol is nonlinear, the flux density response due to T consists of a fundamental component \tilde{B} and higher harmonics. For minor loop excursions, where |T| is relatively small, \tilde{B} dominates and

$$B \approx \tilde{B} + B_0 = |B|e^{j\phi_B} + B_0 \tag{3}$$

where |B| is the flux density amplitude of the fundamental component, B_0 is the bias flux density, and ϕ_B is the phase of the flux density signal. Hence, the piezomagnetic coefficient $d_{33}^I = |B|/|T|$ and the hysteresis in d_{33}^I are quantified in terms of $\Delta\phi_{BT} = \phi_B - \phi_T$. Fig. 1 shows a small discrepancy between the flux density versus stress curve described by (2) and (3) and the actual measurement.

2) Loss Factor η : The hysteresis energy loss was quantified in terms of the area enclosed by the stress–flux density loops [12]. Recent studies have calculated the loss factor of magnetostrictive materials in the frequency domain [33]. By ignoring the higher harmonics the strain due to the sinusoidal stress T is

$$S \approx |S|e^{j\phi_S} + S_0 \tag{4}$$

where |S| is the strain amplitude of the fundamental component, S_0 is the strain due to the static stress, and ϕ_S is the phase of the strain. The system loss factor η is

$$\eta = \tan(\Delta\phi_{ST}) = \tan(\phi_S - \phi_T) \tag{5}$$

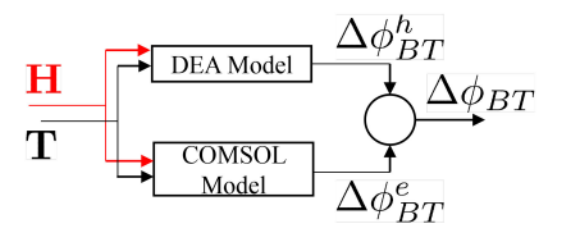


Fig. 2. Flowchart of the material-level model for Galfenol.

where $\Delta\phi_{\rm ST}$ denotes the phase difference between the corresponding strain and the input stress.

B. Model Formulation

1) Material-Level Model Describing d_{33}^I : The material-level model describes the magnetomechanical coupling of magnetostrictive materials by taking boundary stress and magnetic field as inputs while calculating the induced magnetic flux density. The phase lag $\Delta\phi_{\rm BT}$, which represents the rate-dependent hysteresis in flux density versus stress curves, consists of two components: the phase lag due to magnetic hysteresis $\Delta\phi_{\rm BT}^h$ and the phase lag due to eddy current loss $\Delta\phi_{\rm BT}^e$. Deng [30] recently developed and validated an analytical material-level model by decoupling magnetic hysteresis and eddy current losses. However, the model assumes no magnetic flux leakage along the radial direction, and only applies to sinusoidal boundary magnetic field excitation.

This study applies the same decoupling concept while implementing the finite element method to calculate magnetic field diffusion. Magnetic flux along both the axial and radial directions in a cylindrical magnetostrictive material can thus be modeled. Values of $\Delta\phi_{\rm BT}^h$ and $\Delta\phi_{\rm BT}^e$ are computed using two separated steps, as shown in Fig. 2. In the first step, the value of $\Delta\phi_{\rm BT}^h$, which is not frequency-dependent, is calculated using the Evans–Dapino discrete energy-averaged (DEA) model [14]. In the second step, the rate-dependent phase lag component $\Delta\phi_{\rm BT}^e$ is described by a two-dimensional (2-D) axisymmetric model in COMSOL Multiphysics, as shown in Fig. 3. Since magnetostriction is not of interest in the material-level model, only the magnetic dynamics is discussed in the finite element framework using the Ampere's law

$$\int_{A_B} r\mathbf{H} \cdot \delta \mathbf{B} dr dz + \int_{A_B} r\sigma \frac{\partial A}{\partial t} \cdot \delta A dr dz$$

$$= \int_{l_B} rH_T \cdot \delta A dl$$
(6)

where A_B denotes the magnetic domain, A is the magnetic vector potential, σ is the electrical conductivity, $\mathbf{H} = [H_r, H_z]^T$ is magnetic field, and $\mathbf{B} = [B_r, B_z]^T$ is magnetic flux density. The symbol H_T denotes the magnetic field on surface l_B , as shown in Fig. 3.

The nonlinear magnetomechanical coupling of Galfenol is described by a lookup table $f_H(\cdot)$ [34], [35]. The corresponding magnetic field in the Galfenol domain is

$$\mathbf{H} = f_H(|\mathbf{B}|, \mathbf{T_t}) \cdot \frac{\mathbf{B}}{|\mathbf{B}|},\tag{7}$$

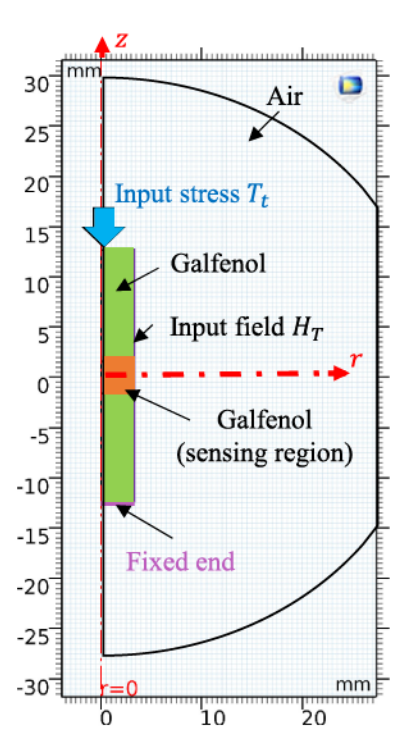


Fig. 3. Geometry of the material-level model in COMSOL Multiphysics.

where T_t is the boundary stress. Ampere's law together with the boundary conditions are calculated using the ac/dc module in COMSOL Multiphysics. Second-order (quadratic) triangular elements are implemented to discretize the system. The bias magnetic flux density is first calculated using a stationary solver. By taking the result of the static solver as initial condition, the dynamic response is then quantified by a Backward Differentiation Formula (BDF) time-dependent solver. At least seven cycles of mechanical stress are applied to ensure the system's eddy currents reach steady state. At least 50 points per cycle are implemented to achieve smooth magnetic flux density versus stress curves. The value of $\Delta \phi^e_{\rm BT}$ is calculated from the phase difference between the average flux density $B_a(t)$ and the average stress $T_a(t)$ within the sensing region.

The final stress-flux density responses are plotted by combining the two phase lag components. The modeled stress T_m and modeled flux density B_m are

$$T_m = |T_a(t)| \cos(2\pi f_0 t) + T_{a0}$$

$$B_m = |B_a(t)| \cos(2\pi f_0 t + \Delta \phi_{BT}^h + \Delta \phi_{BT}^e) + B_{a0}$$
(8)

where T_{a0} and B_{a0} are the constant offsets of $T_a(t)$ and $B_a(t)$ extracted from the COMSOL modeling results, respectively.

2) System-Level Model Describing η : The material-level model is able to reproduce the rate-dependent and nonlinear behavior of magnetostrictive materials when the applied magnetic field and mechanical stress are given. In magnetostrictive dampers or other magnetostrictive systems, the magnetic biasing is provided by permanent magnets and the magnetic field on the surface of the magnetostrictive element is not always directly measured. Hence, the system-level model presented in Fig. 4 is developed. In this study, magnetostrictive dampers are investigated and thus only the phase lag between induced strain

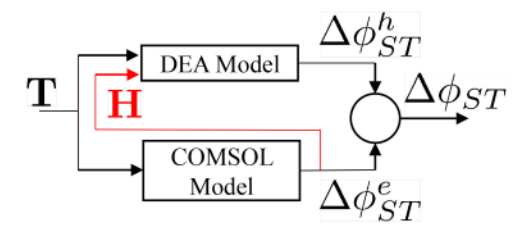


Fig. 4. Flowchart of the system-level model for Galfenol.

and stress is simulated. The same algorithm is also capable of modeling magnetic flux density versus stress curves when the boundary magnetic field is not directly measured. The phase lag $\Delta\phi_{\rm ST}$ consists of the hysteresis component $\Delta\phi_{\rm ST}^h$ and eddy current component $\Delta\phi_{\rm ST}^e$. Similar to the material-level model, the value of $\Delta\phi_{\rm ST}^h$ is calculated by the DEA model, requiring knowledge of the boundary magnetic field H_T .

The boundary field \mathbf{H}_T depends on the mechanical and magnetic domains. Hence, an additional solid mechanics module is added to the finite element framework. The governing equation describing the mechanical dynamics in the system-level finite element model is derived from Newton's law [1]

$$\int_{A_u} r(\mathbf{T} \cdot \delta \mathbf{S}) dr dz + \int_{A_u} r \rho \frac{\partial^2 \mathbf{u}}{\partial t^2} \cdot \delta \mathbf{u} dr dz = \int_{l_u} r \mathbf{T}_t \cdot \delta \mathbf{u} dl$$
(9)

where A_u denotes the mechanical domain, ρ is the material density, and u is the displacement field. The stress–strain relationship can be estimated by a linear function for elastic and passive materials. For magnetostrictive materials, however, the magnetic response affects the mechanical system, resulting in a field-dependent Young's modulus. The varying Young's modulus E_G and the resulting nonlinear stress–strain relationship are described by a lookup table as

$$E_G = f_E(|\mathbf{B}|, \mathbf{T_t}) \tag{10}$$

where the nonlinear 2-D function $f_E(\cdot)$ is calculated from the DEA model.

The magnetic dynamics is described by Ampere's law

$$\int_{A_{R}} r\mathbf{H} \cdot \delta \mathbf{B} dr dz + \int_{A_{R}} r\sigma \frac{\partial A}{\partial t} \cdot \delta A dr dz = 0.$$
 (11)

The boundary condition for the permanent magnet domain A_M is

$$\mathbf{B}|_{A_M} = \mathbf{B}_f \tag{12}$$

where \mathbf{B}_f is the remanent flux density of the magnets. A constant magnetic permeability is able to describe the linear field–flux density relationship in passive magnetic materials. For magnetostrictive materials, the mechanical excitation influences the magnetic response by introducing stress-dependent magnetic permeability. The varying permeability and the resulting nonlinear field–flux density relationship are described by (7).

Second-order triangular elements together with a BDF timedependent solver are implemented to solve the fully coupled system-level model. The total loss factor associated with the

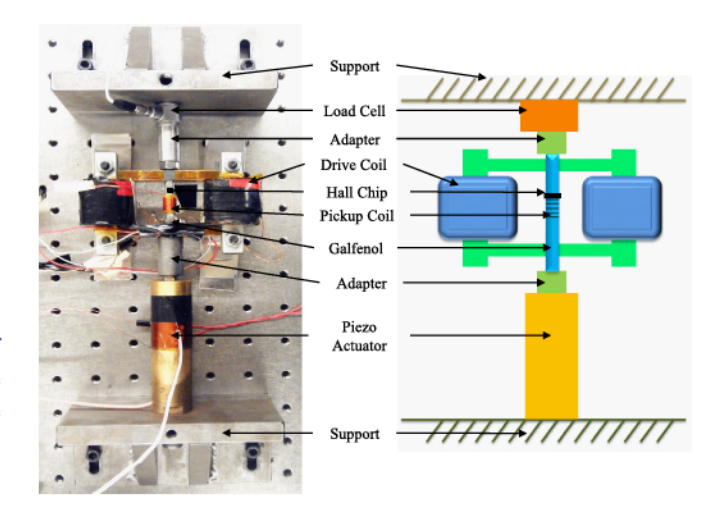


Fig. 5. Galfenol device employed for characterization of dynamic minor loops.

system is

$$\eta = \tan(\Delta \phi_{ST}^h + \Delta \phi_{ST}^e). \tag{13}$$

III. MATERIAL-LEVEL MODEL VALIDATION

A. Experimental Setup

A research grade, <100>-oriented, highly textured, polycrystalline Fe_{81.6}Ga_{18.4} Galfenol rod, produced by ETREMA Products, Inc., was characterized. The sample was 6.35 mm (0.25 inch) in diameter and 73.66 mm (2.9 inch) in length. The electromagnetic transducer used to generate the bias magnetic field through the sample consisted of a pair of electromagnets and an O-shaped magnetic flux path (Fig. 5). The flux path was formed by laminated magnetic steel, thus its magnetic reluctance and eddy current loss were negligible. Flux density was measured by using a custom pick-up coil (70-turn) located in the middle of the rod and a Walker Scientific MF-5D integrating fluxmeter. An Allegro A1301KUA-T Hall chip was installed to measure the magnetic field on the surface of the rod. The dynamic mechanical loading was applied by a PSt-1000/16-VS-25 Piezo actuator (APC International), which was driven by a piezomechanik RCV-1000/7 high power switching amplifier. A PCB208C02 load cell was utilized to measure the dynamic axial load applied on the Galfenol rod. The amplitude of the varying stress was tuned to 3 \pm 0.2 MPa by manually adjusting the voltage amplitude applied to the piezo actuator. As the mechanical excitation approaches the fundamental frequency of the system, the entire Galfenol rod vibrates against the load cell while experiencing no significant mechanical stress. The first mode of the experimental setup is dominated by the relatively low stiffness of the load cell. Due to the Delta-E effect of Galfenol, the fundamental frequency also varies with respect to the excitation current and bias mechanical stress. To simplify the discussion, the lower bound of the first resonant frequency was estimated by assuming a constant Young's modulus of 32.5 GPa for Galfenol, which is the minimum value observed in a previous study [3]. An eigenfrequency study conducted in COMSOL Multiphysics showed that the first mode of the setup is around 1 kHz. Hence,

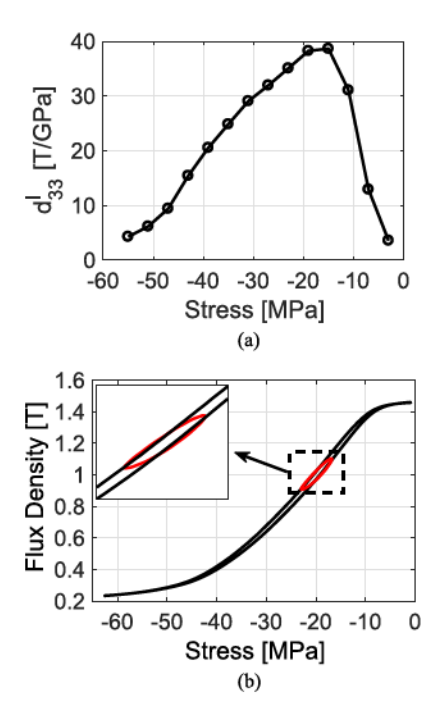


Fig. 6. (a) Piezomagnetic coefficient d_{33}^I versus stress for 500 mA constant current measurement at 0.05 Hz. (b) Flux density versus stress, major and minor loops comparison. Major loop (black line): 500 mA constant current, 0.05 Hz; minor loop (red line): 500 mA constant current, 4 Hz.

the maximum frequency of mechanical excitation is limited to 800 Hz.

The constant current flux density versus stress loops have been measured by Weng et al. [19] for the same sample in the quasi-static regime, and the maximum d_{33}^{I} was observed at a 500 mA bias current and a -20 MPa bias stress [Fig. 6(a)]. The same optimal bias position was utilized in this study. The bias current was provided by an Agilent power supply; the bias stress was first coarsely adjusted by changing the distance between two supports and then fine-tuned by modifying the voltage offset on the piezo actuator. However, the static bias stress measurement was not straightforward in this study, since the PCB load cell is only able to measure the dynamic force. Furthermore, adding another static load cell in series greatly increased system compliance and reduced system natural frequency. A previous study [19] has proven that the quasi-static minor loops are enclosed by the major loops at the same bias field/current. Hence, in this study, the optimal bias stress (about −20 MPa) was achieved by tuning the dc voltage offset across the piezo actuator until the flux density versus stress minor loop fell within its corresponding major loop, as shown in Fig. 6(b). This technique could bring the bias stress close enough to the optimal location, since the quasi-static d_{33}^I of 32.27 T/GPa observed in this study matches previous results [19].

B. Results

The minor loops were measured at stress frequencies ranging from 4 Hz to 800 Hz. Initially, the input forcing frequency was 4 Hz, followed by frequencies from 10 to 100 Hz in 10 Hz steps.

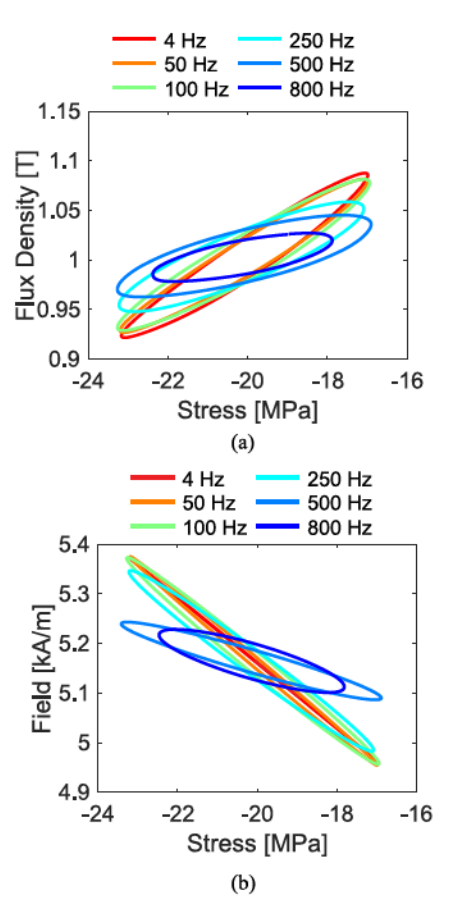


Fig. 7. (a) Flux density versus stress minor loops and (b) field versus stress minor loops at 4, 50, 100, 250, 500, and 800 Hz.

The increment was then changed to 25 Hz for input frequencies ranging from 100 to 300 Hz, and 50 Hz for the input frequencies above 300 Hz. The initial frequency was selected as 4 Hz, which could be assumed as quasi-static, for consistency with relevant work on Terfenol-D [2] and Galfenol [19] in the literature.

Fig. 7(a) presents the rate-dependent flux density versus stress minor loops at selected frequencies. As the excitation frequency increases, the flux density versus stress minor loops rotate clockwise, which implies a decreasing d_{33}^{I} value. The stress amplitude |T| is manually tuned by changing the voltage into the piezo actuator thus having an absolute error of 0.2 MPa. At 800 Hz, the stress amplitude barely falls within error limits, when the maximum voltage available from the amplifier (0-1000 V) is applied to the piezo actuator, because the excitation frequency is close to the mechanical resonance. The magnetic field measured on the rod's surface is presented in Fig. 7(b). Since the permeability of Galfenol is stress-dependent [15], the magnetic field through Galfenol varies with respect to applied stress. The field versus stress minor loops rotate counterclockwise, which indicates that the permeability variation in Galfenol reduces as excitation frequency increases.

The rate-dependent d_{33}^I and $\Delta\phi$ are presented in Fig. 8(a) and (b), respectively. Both d_{33}^I and $\Delta\phi$ decrease monotonically with respect to the excitation frequency. The drop of both variables becomes significant above 100 Hz. The steep increment in hysteresis and the reduction in magnetomechanical coupling at high

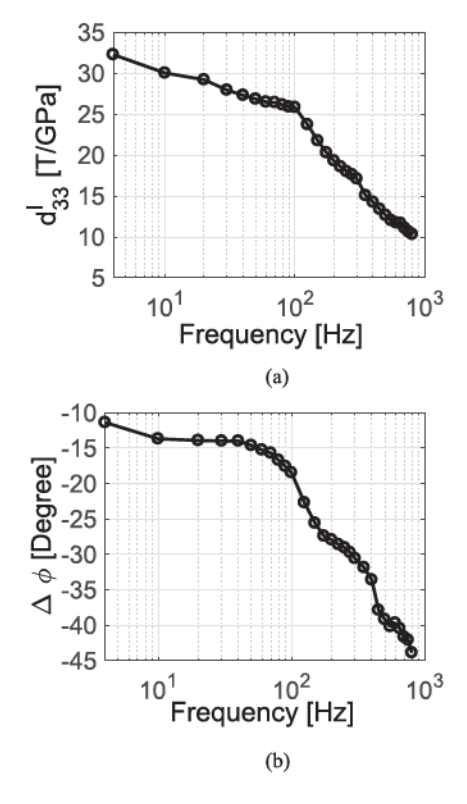


Fig. 8. (a) Piezomagnetic coefficient d_{33}^I and (b) phase lag $\Delta\phi$ with respect to frequency of dynamic force (from 4 Hz to 800 Hz).

frequency are mainly due to the eddy current loss induced by the dynamic stress. The cutoff frequency of 100 Hz observed in this study fits the numerical prediction in a previous study [10]. Overall, d_{33}^I decreases from 32.27 T/GPa to 10.33 T/GPa and $|\Delta\phi|$ increases from 11.38° to 43.87° over the frequency range of 4–800 Hz.

Fig. 9 presents the modeling result at selected driving frequencies. Under 4 Hz sinusoidal stress excitation, the eddy current effect is negligible and thus the hysteresis is all due to the pinning site loss. The stress–flux density curve at 4 Hz gives a $\Delta\phi_p$ of $-14^\circ.$ The derived model is able to describe the increment of hysteresis size and reduction of piezomagnetic constant with respect to excitation frequency.

IV. MAGNETOSTRICTIVE DAMPER DESIGN

A. Configuration

Taking advantage of mechanically induced eddy current loss and magnetic hysteresis loss, a conceputal design of magnetostrictive dampers is proposed in this study, as shown in Fig. 10. A <100>-oriented, highly textured, polycrystalline ${\rm Fe_{81.6}Ga_{18.4}}$ rod with a radius of 3 mm and a length of 9.5 mm is implemented. The performance of this Galfenol rod depends on stress biasing and magnetic biasing. A disk spring is used to provide the bias stress on the Galfenol rod. The bias stress can be manually tuned by threading the cap into the case. The Galfenol rod and the output shaft made of stainless steel 316 are in flat contact. Thus, this device only takes purely axial load. Due to the machinability of Galfenol, future devices can pos-

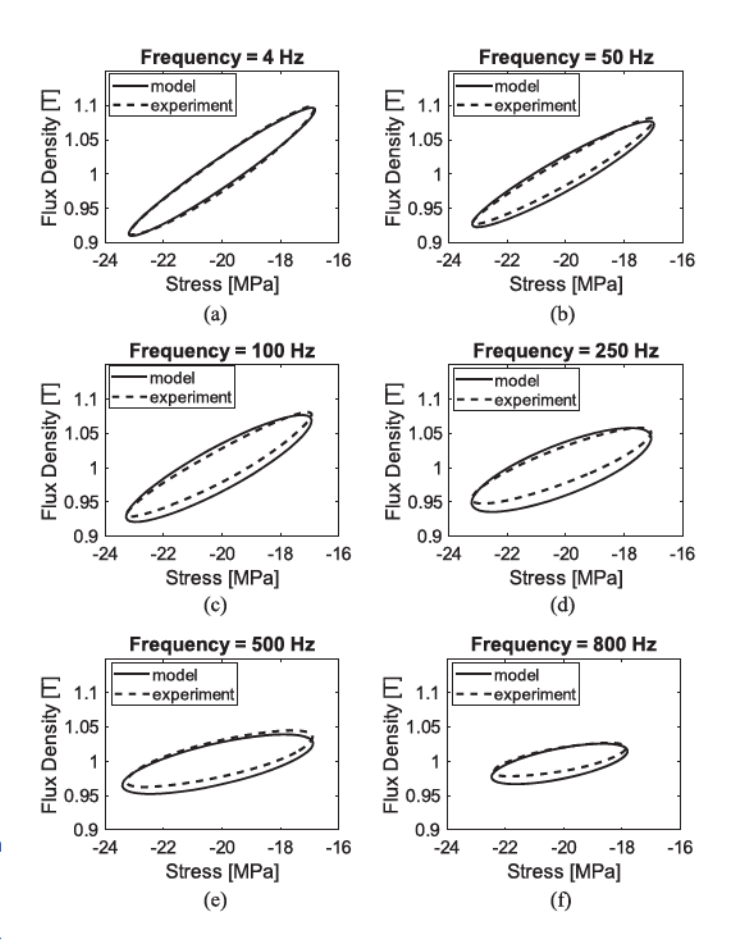


Fig. 9. Results of the material-level model at selected excitation frequencies.

sibly take bending or torsional loads. The magnetic biasing is provided by a cylindrical Alnico magnet, whose remanent flux density is 0.6 T. Two soft iron plates are inserted to prevent magnetic flux density leakage. Deng and Dapino [11] showed that adding a flux path in parallel to the Galfenol rod improves the magnetomechanical coupling when Galfenol is biased by permanent magnets. Hence, a ring-shaped flux path made of 1006 low carbon steel is placed between the magnet and the Galfenol rod. The flux path is laminated to eliminate the eddy current loss. The 2-D axisymmetric geometry as well as dimensions of each component is presented in Fig. 10(b). The cap, the case, and the base are ignored in COMSOL Multiphysics due to the negligible magnetic flux density variations in these components.

A 280 N amplitude, 750 Hz sinusoidal force is applied on the output shaft along the axial direction. The system loss factor is estimated using the system-level model developed in this study. System optimization is conducted by tuning the bias stress T_0 , the thickness of the flux path T_p , and the thickness of the cylindrical magnet T_m .

B. Results

1) Loss Factor η —No Flux Path: Fig. 11 shows the loss factor as a function of T_0 and T_m , when no flux path is utilized. The bias stress T_0 sweeps from -60 MPa to 0 MPa in 5 MPa steps; the permanent magnet thickness T_m sweeps from 0.25 mm to

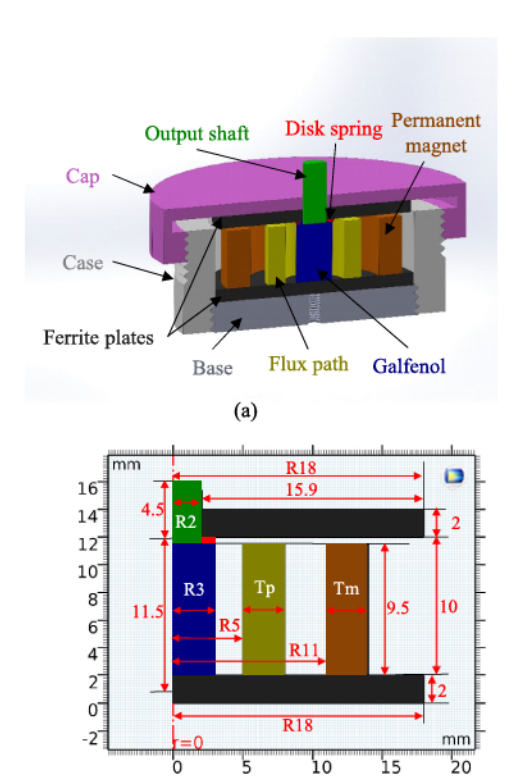


Fig. 10. (a) 3-D assembly of a conceptual magnetostrictive damper and (b) dimensions of the magnetostrictive damper where the air domain is neglected for clarity.

(b)

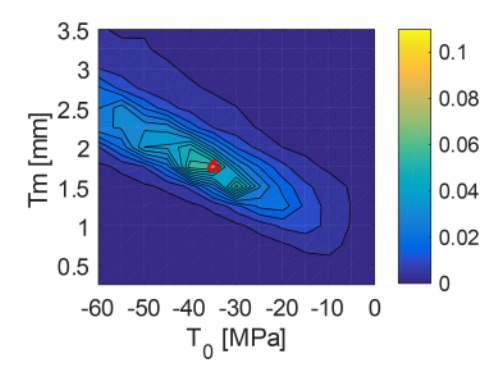


Fig. 11. Loss factor of the magnetostrictive damper without magnetic flux path, where the red triangle indicates the peak of the loss factor simulation.

 $3.5~\mathrm{mm}$ in $0.25~\mathrm{mm}$ steps. Two saturation regions exist where the loss factor is negligible. When the permanent magnet is large, which corresponds to the top right corner in Fig. 11, Galfenol is saturated by the applied magnetic field, thus the flux density variation and the loss factor are almost 0. When the mechanical stress is large, which corresponds to the bottom left corner in Fig. 11, the stress forces all magnetic domains to the basal plane and thus the loss factor also becomes 0. When applied magnetic energy and mechanical energy are balanced, the magnetomechanical coupling is highest. As the thickness of permanent magnet T_m increases, a large compression stress is required to

match the magnetic field energy. A maximum loss factor of 0.059 is achieved, when $T_m=1.75~\mathrm{mm}$ and $T_0=-35~\mathrm{MPa}$.

2) Loss Factor η —Flux Path: Deng and Dapino [9], [11] have theoretically and experimentally proven that the piezomagnetic coefficient d_{33}^{ϕ} of Galfenol, which quantifies the magnetomechanical coupling, can be improved by placing a magnetic flux path between the cylindrical magnet and the Galfenol rod. Fig. 12 presents the loss factor of the magnetostrictive damper versus T_0 and T_m when different flux paths are installed. The thickness of the magnetic flux path T_p changes from 1 mm to 5 mm in 1 mm steps. The optimal values of T_0 and T_m that result in the maximum loss factor are summarized in Table I.

Three observations can be made as follows:

- The optimal T_m increases as T_p increases.
- The loss factor becomes less sensitive to T_p when $T_p > 2$ mm.
- The optimal $|T_0|$ increases as T_p decreases.

The loss factor of the magnetostrictive damper is optimal when two conditions are satisfied: a) the magnetostrictive material operates in the burst region where the piezomagnetic coefficient and the magnetic permeability are maximum and b) the magnetic reluctance of the flux path R_p equals the magnetic reluctance of the magnetostrictive material R_G . The value of R_G , which is determined by μ , is stress- and field-dependent. Fig. 13 shows that the magnetic permeability measured from a polycrystalline ${\rm Fe_{81.6}Ga_{18.4}}$ rod. The peak value of μ decreases from 690 to 192, as T_0 varies from -1.64 MPa to -61.31 MPa. Hence, the magnetic reluctance R_G increases from $\min(R_G)$ to $\max(R_G)$ with respect to an increasing $|T_0|$. The three aforementioned observations can be explained as follows:

- For a given bias stress T_0 , the optimal strength of permanent magnets that biases the magnetostrictive material at the burst region is fixed. As the value of T_p increases, more magnetic flux leaks through the flux path, and thus a larger T_m is required.
- When $T_p < 2$ mm and $R_p > \max(R_G)$, R_p cannot match R_G . One of the aforementioned optimal conditions cannot be satisfied and thus the loss factor is relatively small. Modeling results in Table I show that the variation of the maximum η is within 3% when $T_p \geq 2$ mm and R_p falls within the range of R_G . Hence, the geometry of the flux path is not critical in system design, once the thickness of the flux path is greater than a certain value. As T_p keeps increasing and $R_p < \min(R_G)$, a reduction of loss factor η is expected. However, this case requires an extremely thick flux path which is not discussed in this study.
- When $T_p \geq 2$ mm and R_p falls within the range of R_G , the optimal loss factor is achieved when $R_p = R_G$. As T_p increases, the value of R_p reduces and thus a smaller R_G is required. According to the stress- and field-dependent μ presented in Fig. 13, R_G is reduced by decreasing $|T_0|$.

Figs. 11 and 12 also demonstrate that the dc component of the mechanical load T_0 can be implemented to adjust the dynamics of the magnetostrictive damper. Due to the stress-dependent material properties, the damper proposed in this study can be adaptive; the loss factor can thus be adjusted continuously from 0 to the maximum value by changing the bias stress.

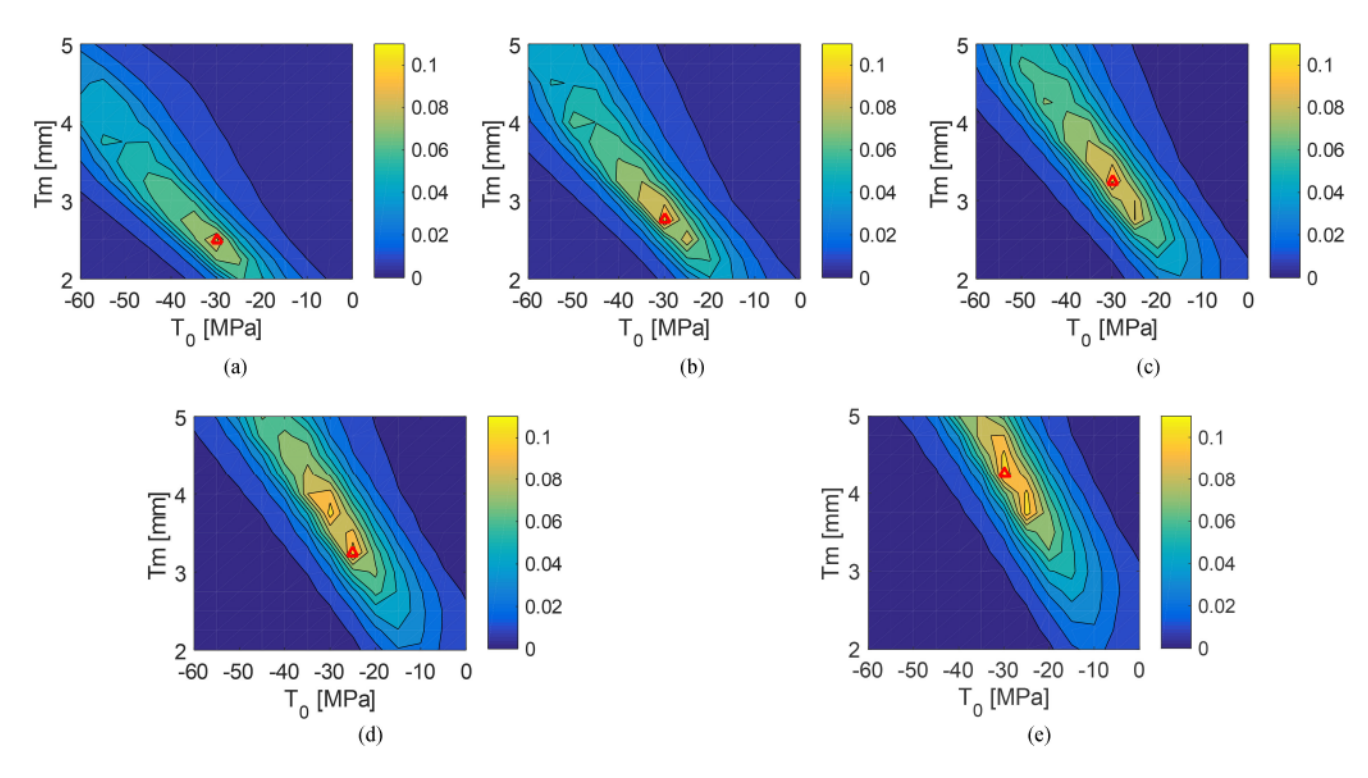


Fig. 12. Loss factor of the magnetostrictive damper under various bias stress T_0 and thickness of the cylindrical permanent magnets T_m : (a) $T_p = 1$ mm, (b) $T_p = 2$ mm, (c) $T_p = 3$ mm, (d) $T_p = 4$ mm, and (e) $T_p = 5$ mm. The red triangular indicates the peak location of the maximum loss factor.

TABLE I MAXIMUM LOSS FACTORS AND ASSOCIATED OPTIMAL BIAS STRESSES AND OPTIMAL PERMANENT MAGNET DIMENSIONS AT GIVEN FLUX PATH THICKNESS

Tp [mm]	0	1	2	3	4	5
Optimal Tm [mm]	1.75	2.5	2.75	3.25	3.25	3.75
Optimal T_0 [MPa]	-35	-30	-30	-30	-25	-25
η [-]	0.059	0.093	0.104	0.104	0.107	0.106

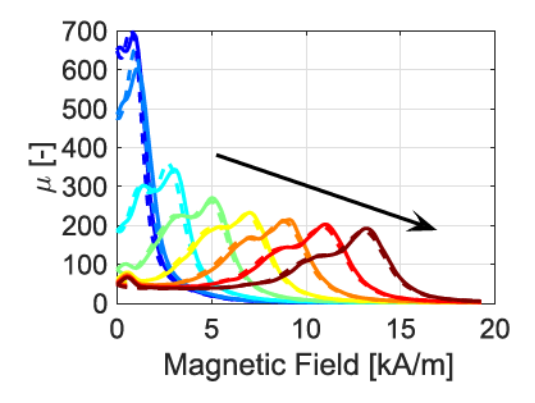


Fig. 13. Relative magnetic permeability μ measured from a <100>-oriented, highly textured, polycrystalline $\mathrm{Fe_{81.6}Ga_{18.4}}$ rod under -1.64, -10.23, -20.44, -30.65, -40.88, -51.10, and -61.31 MPa bias stress at 4 Hz. Arrow indicates the increasing of bias stress.

V. CONCLUSION

This study demonstrates that the hysteresis loss and eddy current loss intrinsic to magnetostrictive materials can be implemented to passive damper design. The rate-dependent energy loss in magnetostrictive materials is first characterized by applying a constant current of 500 mA on a pair of electromagnets. The stress-induced eddy current loss and its influence

on piezomagnetic coefficient d_{33}^{I} are quantified using flux density versus stress curves measured from a research grade, <100>-oriented, highly textured, polycrystalline Fe_{81.6}Ga_{18.4} Galfenol rod subjected to a dynamic mechanical loading from 4 to 800 Hz. The value of d_{33}^I monotonically reduces, especially after the cutoff frequency of about 100 Hz, from 32.27 T/GPa to 10.33 T/GPa. The intrinsic energy loss is evaluated in terms of the phase lag of the flux density relative to the input stress. The value of $|\Delta\phi|$ increases from 11.38° to 43.87° over the full frequency range. A material-level model based on the finite element method is able to track both piezomagnetic coefficient reduction and hysteresis increment up to 800 Hz. The experimental and modeling results prove that stressinduced eddy current loss and magnetic field diffusion greatly reduces magnetomechanical coupling strength in monolithic Galfenol.

Taking advantage of the mechanically induced eddy current loss and magnetic hysteresis loss, this study designs a coil-less, solid-state, and adaptive magnetostrictive damper, which mainly consists of a cylindrical permanent magnet, a magnetostrictive element, a precompression mechanism, and a predesigned magnetic flux path. The bias stress, as well as the geometries of the permanent magnets and the flux path, is optimized to maximize the system loss factor. Modeling results show that the loss factor can be continuously tuned from 0 to 0.107 by adjusting the precompression.

REFERENCES

 S. Chakrabarti and M. J. Dapino, "A dynamic model for a displacement amplified magnetostrictive driver for active mounts," *Smart Mater. Struct.*, vol. 19, no. 5, 2010, Art no. 055009.

- [2] R. Kellogg and A. Flatau, "Experimental investigation of Terfenol-d's elastic modulus," J. Intell. Mater. Syst. Struct., vol. 19, no. 5, pp. 583– 595, 2008.
- [3] Z. Deng, J. J. Scheidler, V. M. Asnani, and M. J. Dapino, "Quasi-static major and minor strain-stress loops in textured polycrystalline Fe81:6Ga18:4 galfenol," J. Appl. Phys., vol. 120, no. 24, 2016, Art no. 243901.
- [4] J. J. Scheidler, V. M. Asnani, and M. J. Dapino, "Vibration control via stiffness switching of magnetostrictive transducers," in *Proc. Int. Soc. Opt. Eng.*, Las Vegas, NV, Mar. 2016, Art no. 979909.
- [5] J. Yoo, A. Murray, and A. B. Flatau, "Evaluation of magnetostrictive shunt damper performance using iron (fe)-gallium (ga) alloy," in *Proc. Int. Soc.* Opt. Eng., San Diego, CA, Mar. 2014, Art no. 90573I.
- [6] J. J. Scheidler and V. M. Asnani, "Validated linear dynamic model of electrically-shunted magnetostrictive transducers with application to structural vibration control," *Smart Mater. Struct.*, vol. 26, no. 3, 2017, Art no. 035057.
- [7] Z. Deng, "Nonlinear modeling and characterization of the Villari effect and model-guided development of magnetostrictive energy harvesters and dampers," Ph.D. dissertation, Mech. Eng., Ohio State Univ., Columbus, OH, 2015.
- [8] V. M. Asnani, Z. Deng, J. J. Scheidler, and M. J. Dapino, "Experimental comparison of piezoelectric and magnetostrictive shunt dampers," in *Int.* Soc. Opt. Eng., Las Vegas, NV, Mar. 2016, Art no. 98010R.
- [9] Z. Deng, V. M. Asnani, and M. J. Dapino, "Magnetostrictive vibration damper and energy harvester for rotating machinery," in *Proc. Int. Soc.* Opt. Eng., San Diego, CA, Mar. 2015, Art no. 94330C.
- [10] J. J. Scheidler and M. J. Dapino, "Mechanically induced magnetic diffusion in cylindrical magnetoelastic materials," *J. Magn. Magn. Mater.*, vol. 397, pp. 233–239, 2016.
- [11] Z. Deng and M. Dapino, "Magnetic flux biasing of magnetostrictive sensors," Smart Mater. Struct., vol. 26, no. 5, 2017, Art no. 055027.
- [12] J. Restorff, M. Wun-Fogle, and E. Summers, "Hysteresis, d₃₃ and d₃₃ of Fe_{81.6} Ga_{18.4} textured polycrystals," *J. Appl. Phys.*, vol. 109, no. 7, 2011, Art no. 07A922.
- [13] TdVib Ilc., "Galfenol," 2017. [Online]. Available: http://tdvib.com/galfenol/. TdVib Ilc. Accessed on: Jul. 19, 2017.
- [14] P. Evans and M. Dapino, "Efficient magnetic hysteresis model for field and stress application in magnetostrictive Galfenol," J. Appl. Phys., vol. 107, no. 6, 2010, Art no. 063906.
- [15] Z. Deng and M. J. Dapino, "Characterization and finite element modeling of Galfenol minor flux density loops," J. Intell. Mater. Syst. Struct., vol. 26, no. 1, pp. 47–55, 2014.
- [16] L. Weng, W. Li, Y. Sun, W. Huang, and B. Wang, "High frequency characterization of Galfenol minor flux density loops," AIP Adv., vol. 7, no. 5, 2017, Art no. 056023.
- [17] J. Atulasimha, A. B. Flatau, and E. Summers, "Characterization and energy-based model of the magnetomechanical behavior of polycrystalline iron-gallium alloys," *Smart Mater. Struct.*, vol. 16, no. 4, 2007, Art no. 1265
- [18] A. Mahadevan, P. Evans, and M. Dapino, "Dependence of magnetic susceptibility on stress in textured polycrystalline Fe_{81.6} Ga_{18.4} and Fe_{79.1} Ga_{20.9} Galfenol alloys," *Appl. Phys. Lett.*, vol. 96, no. 1, 2010, Art no. 012502.
- [19] L. Weng, T. Walker, Z. Deng, M. Dapino, and B. Wang, "Major and minor stress-magnetization loops in textured polycrystalline Fe_{81.6} Ga_{18.4} Galfenol," *J. Appl. Phys.*, vol. 113, no. 2, 2013, Art no. 024508.

- [20] J. J. Scheidler, V. M. Asnani, and M. J. Dapino, "Frequency-dependent, dynamic sensing properties of polycrystalline Galfenol (Fe_{81.6} Ga_{18.4})," *J. Appl. Phys.*, vol. 119, no. 24, 2016, Art no. 244902.
- [21] M. Al Janaideh, S. Rakheja, and C.-Y. Su, "An analytical generalized Prandtl-Ishlinskii model inversion for hysteresis compensation in micropositioning control," *IEEE/ASME Trans. Mechatronics*, vol. 16, no. 4, pp. 734–744, Aug. 2011.
- [22] H. Janocha, D. Pesotski, and K. Kuhnen, "FPGA-based compensator of hysteretic actuator nonlinearities for highly dynamic applications," *IEEE/ASME Trans. Mechatronics*, vol. 13, no. 1, pp. 112–116, Feb. 2008.
- [23] U. X. Tan, W. T. Latt, C. Y. Shee, C. N. Riviere, and W. T. Ang, "Feedforward controller of ill-conditioned hysteresis using singularityfree Prandtl–Ishlinskii model," *IEEE/ASME Trans. Mechatronics*, vol. 14, no. 5, pp. 598–605, Oct. 2009.
- [24] W. D. Armstrong, "An incremental theory of magneto-elastic hysteresis in pseudo-cubic ferro-magnetostrictive alloys," J. Magn. Magn. Mater., vol. 263, no. 1, pp. 208–218, 2003.
- [25] P. Evans and M. Dapino, "State-space constitutive model for magnetization and magnetostriction of Galfenol alloys," *IEEE Trans. Magn.*, vol. 44, no. 7, pp. 1711–1720, Jul. 2008.
- [26] P. Weetman and G. Akhras, "A three dimensional rate equation model for the dynamical sensing effect of magnetostrictive Galfenol," *J. Appl. Phys.*, vol. 109, no. 4, 2011, Art no. 043 902.
- [27] H. Xu, Y. Pei, D. Fang, and S. Ai, "An energy-based dynamic loss hysteresis model for giant magnetostrictive materials," *Int. J. Solids. and Struct.*, vol. 50, no. 5, pp. 672–679, 2013.
- [28] L. Weng, Q. Zhao, Y. Sun, W. Huang, B. Wang, and S. Busbridge, "Dynamic experiments of strain and magnetic field for Galfenol rod and its modeling," *IEEE Trans. Appl. Supercond.*, vol. 26, no. 4, Jun. 2016, Art no. 0600605.
- [29] Z. Li, X. Zhang, G. Gu, X. Chen, B. Wang, and C. Su, "A comprehensive dynamic model for magnetostrictive actuators considering different input frequencies with mechanical loads," *IEEE Trans. Ind. Informat.*, vol. 12, no. 3, pp. 980–990, Jun. 2016.
- [30] Z. Deng, "Dynamic discrete energy-averaged model for magnetostrictive materials," J. Magn. Magn. Mater., vol. 441, pp. 757–763, 2017.
- [31] X. Zhao and D. Lord, "Application of the Villari effect to electric power harvesting," J. Appl. Phys., vol. 99, no. 8, 2006, Art no. 08M703.
- [32] ASTM Stardards D5992-96, 2011, "Standard guide for dynamic testing of vulcanized rubber and 618 rubber-like materials using vibratory methods," ASTM International, West Conshohocken, PA, 2011, doi: 10.1520/D5992-96R11.
- [33] J. J. Scheidler, V. M. Asnani, and M. J. Dapino, "Dynamically tuned magnetostrictive spring with electrically controlled stiffness," *Smart Mater. Struct.*, vol. 25, no. 3, 2016, Art no. 035007.
- [34] Z. Deng and M. J. Dapino, "Modeling and design of Galfenol unimorph energy harvesters," Smart Mater. Struct., vol. 24, no. 12, 2015, Art no. 125019.
- [35] Z. Deng and M. J. Dapino, "Influence of electrical impedance and mechanical bistability on Galfenol-based unimorph harvesters," J. Intell. Mater. Syst. Struct., 2016, Art no. 1045389X16666176.

Authors' photographs and biographies not available at the time of publication.